

## Corrosion behaviors of 3-D printed Ni-based alloy in molten NaCl–MgCl<sub>2</sub> salt

Younghwan Jeon, Hyeongjin Byeon, Kiwon Kang, Jaeyeong Park\*

Department of Nuclear Engineering, Ulsan National Institute of Science and Technology,  
50 UNIST-gil, Ulju-gun, Ulsan 44919, Republic of Korea

\*Corresponding author: jypark@unist.ac.kr

### 1. Introduction

Molten salt is used for solar power generation and energy storage based on various advantages such as high thermal conductivity, heat capacity, boiling temperature, and no reactivity in air. In particular, molten salt reactors (MSR) are being actively developed due to advantages such as irradiation resistance and neutronic benefits. The biggest concern of the molten salt-based technology is molten salt-induced corrosions, and various studies are also underway to develop alloys that can withstand harsh corrosive condition. Recent studies in the fields of solar power generation and energy storage, it is evaluated that alloys such as stainless steel and Ni-based alloy have molten salt corrosion resistance as needed. However, in the case of MSR, the corrosion condition is very strong due to various fissile elements and fission products dissolved in the salt, and for this reason, Ni-based alloy is considered the most-promising alloy. [1, 2]

The corrosion behavior of alloys in a molten salt environment has mainly been evaluated only for castings. Apart from this, metallic 3-D printing has undergone extraordinary technological development over the past 10 years, and mechanical, thermal properties and economic aspects of these 3-D print-based components have been thoroughly evaluated. [3, 4] However, 3-D printed products has some disadvantages that are vulnerable to molten salt-induced corrosion, such as micro-grains and printing interfaces. Therefore, the application of 3-D printed products in the molten salt-based energy industry are not widely researched. In other words, the corrosion behaviors of 3-D printed products in molten salt system have not yet been well-announced. Therefore, in order to apply 3-D printed products to the molten salt application, it is necessary to evaluate the corrosion characteristics of 3-D printed products compared to castings.

In this paper, the 80Ni–20Cr alloy was fabricated using casting and DED-type 3-D printing. In particular, the corrosion behaviors of 3-D printed product before and after the heat treatment was studied. The corrosion behavior of the alloy was analyzed by observing the microstructural changes of the specimen before and after the corrosion test through SEM–EBSD–EDS and OM. Salt composition change was traced by using ICP–OES. Based on these results, it was suggested whether the 3-D printed product can be applied to the molten salt application

### 2. Experimental setup

#### 2.1. Specimen preparation

It is well known that certain elements or compounds in alloys can accelerate or decelerate molten salt corrosion. The aim of this study is the corrosion behavior analysis of 3-D printed products in a molten salt system, so 80Ni–20Cr, which is an alloy of noble element (Ni) and reactive element (Cr), was selected as the target alloy. 80Ni–20Cr alloy plate was produced using casting and 3-D printing technology. The traditional alloy sheet was produced by casting and hot-rolled at 1200 °C condition.

The metallic powder for 3-D printing was manufactured to have a composition of 80Ni–20Cr using the gas atomization technique and sieved to collect 50–100 μm-sized particles. The black spots observed on the powder surface in Figure 1 (b) are Cr<sub>2</sub>O<sub>3</sub>, which are presumed to have been caused by exposure to the air during the transportation process. However, the contents of carbon and oxygen were identified as less than 500 ppm by using an element analyzer.

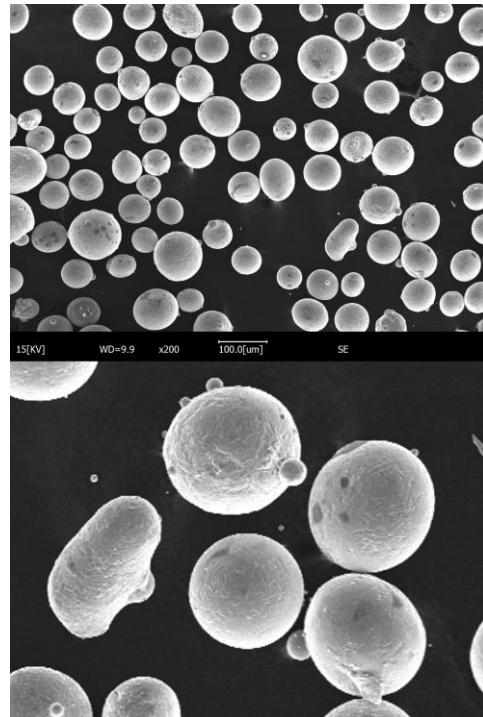


Figure 1. SEM images of 3-D printing powder

3-D printed 80Ni–20Cr sheet was produced using DED-type 3-D printer. The product was produced in the form of a sheet with a size of 80x40x3.2 mm. The laser beam spot size was 800  $\mu\text{m}$  and the z-axis step size was set to 200  $\mu\text{m}$ . The direction of nozzle movement of the 3D printer and fabricated product are shown in Fig. 2. Laser power was set to 375 W, 10 L/min of Ar gas (99.996%) flow rate, and 2.8 g/min of powder feed rate was adjusted. The product was separated from the substrate using electrical discharge machining and separated into a sheet form, and the surface valleys generated during the 3-D printing process were removed by polishing at room temperature. The composition of the 3-D printed 80Ni–20Cr sheet was confirmed by using ICP–OES and Element analyzer.

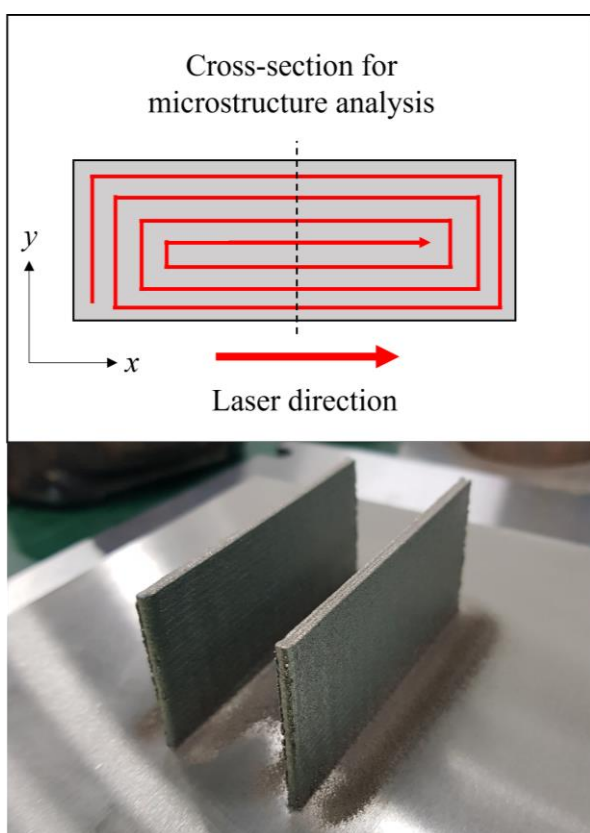


Figure 2. Nozzle direction during printing (top) and as-fabricated product (bottom)

The specimen for the corrosion experiment was cut by using a waterjet (T500 3015 hybrid, TOPS) to minimize specimen damage. Heat treatment was performed for 3-D printed products using an electrical furnace that can maintain inert Ar condition. Since there is no transformation–time–temperature diagram data for the 80Ni–20Cr alloy, heat treatment was performed under the heat treatment conditions of Inconel 600, which has a similar composition among the commercial Ni-based alloys. Specifically, solutionising at 1000  $^{\circ}\text{C}$  for 1 hour and ageing at 750  $^{\circ}\text{C}$  for 8 hours were conducted. Afterward, the surface of the specimen was polished with sandpaper and 1  $\mu\text{m}$   $\text{Al}_2\text{O}_3$ .

## 2.2. Corrosion cell

NaCl (99.99%, Alfa Aesar) and  $\text{MgCl}_2$  (99.99%, Alfa Aesar) were used as corrosive salt and were sequentially heated for 24 hours in an environment of 200  $^{\circ}\text{C}$ , 400  $^{\circ}\text{C}$ , and 600  $^{\circ}\text{C}$  to remove residual moisture and oxygen from the salt. The salt was mixed with a eutectic composition of 58.0 at.% NaCl–42.0 at.%  $\text{MgCl}_2$  and heated at 600  $^{\circ}\text{C}$  for 24 hours. The salt was taken out and solidified to use as a salt reagent. As a result of ICP–OES analysis on the salt, it was confirmed that the Na: Mg ratio satisfies the eutectic standard.

A BN crucible with an inner diameter of 24 mm and height of 30 mm was used for the corrosion cell and a stopper was used to prevent external foreign matter contaminants during the corrosion experiments. The metal specimen was held through the small holes on the stopper and adjusted so that it did not touch the bottom of the cell. For each corrosion experiment, 15.000 g of NaCl– $\text{MgCl}_2$  salt was loaded.

All corrosion experiments were performed in a glove box where moisture and oxygen concentrations were kept below 0.1 ppm. Reagent preparation and corrosion experiments were conducted in a PID electrical furnace attached to a glove box that has a temperature accuracy of  $\pm 0.1$   $^{\circ}\text{C}$ . During the experiment, a dummy cell filled with the same amount of NaCl– $\text{MgCl}_2$  with the corrosion test was installed in the center of the furnace to monitor the temperature.

## 2.3. Experimental setup

80Ni–20Cr alloys fabricated by casting and 3-D printing were corroded for 1, 3, 7, and 28 days in a molten NaCl– $\text{MgCl}_2$  salt at 700  $^{\circ}\text{C}$ . Specimen made by casting, as-fabricated 3-D printed specimen, and thermally treated 3-D printed specimen was weighed using an electronic scale before the corrosion experiments. After the experiment, the specimen was taken out of the salt and rinsed with distilled water and ultrasonic cleaner, and the moisture of the specimen was removed in a vacuum chamber to prevent oxidation, and the weight of the specimen was measured. After the end of the experiment, the salt was solidified and collected for ICP–OES analysis.

## 2.4. Microstructure characterization

Specimens before and after the corrosion experiments were cut by using a low-speed saw with a direction which is perpendicular to the printing direction (Fig. 2). Cut specimen was hot mounted with conductive resin, and the samples were finally polished by vibration grinding with 0.05  $\mu\text{m}$   $\text{Al}_2\text{O}_3$  paste, and dried in a vacuum chamber to remove infiltrated moisture, and stored in Ar environment. SEM–EBSD–EDS (Quanta 3D FIB, FEI) and OM analysis were performed on the specimen.

### 3. Results and Discussion

#### 3.1. Microstructure analysis

OM and EBSD analyses were performed on conventionally produced and 3-D printed products. As shown in Fig. 3 (b, c), heat treatment allowed the recrystallization of the grains, but micro-grains along the printed layer remain in their original condition. This phenomenon was also observed in EBSD images (Fig. 4 (b–e)). Before the heat treatment, grain orientations are arranged in a random direction (Fig. 4 (b, c)), but, it can be seen that the direction of the grains is constantly aligned after the heat treatment. However, the area where the micro grains were positioned still remained their random orientation. In other words, the annealing effect is expected to be insignificant to the micro grains along the printed layer.

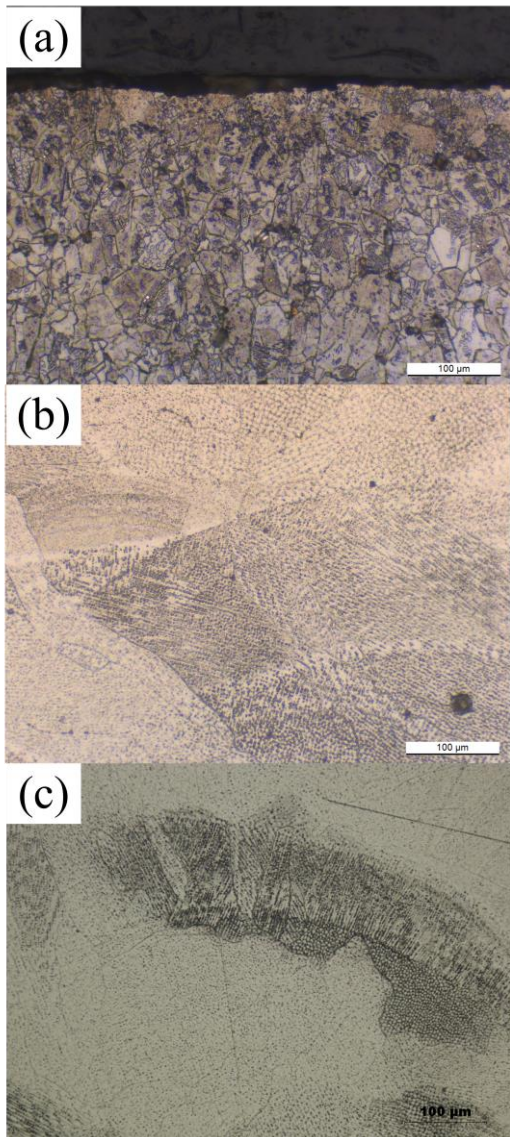


Figure 3. Optical microscope images of 80Ni–20Cr alloy fabricated by casting (a), 3-D printing without heat treatment (b) and with heat treatment (c)

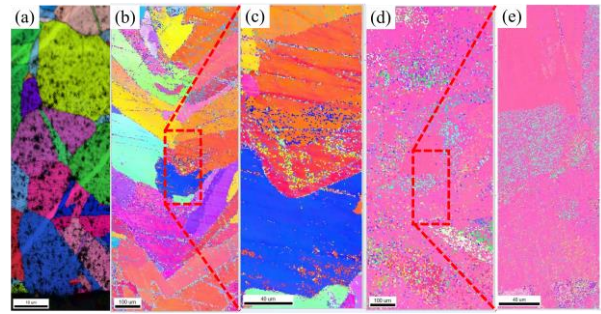


Figure 4. Inverse pole figure (IPF) images of 80Ni–20Cr alloy fabricated by casting (a), 3-D printing without heat treatment (b, c), and with heat treatment (d, e)

#### 3.2. Corrosion behaviors analysis

Corrosion experiments were conducted for 1, 3, 7, and 28 days for each specimen. As shown in Fig. 4, molten salt corrosion was observed, and its depth was analyzed as about 30  $\mu\text{m}$ .

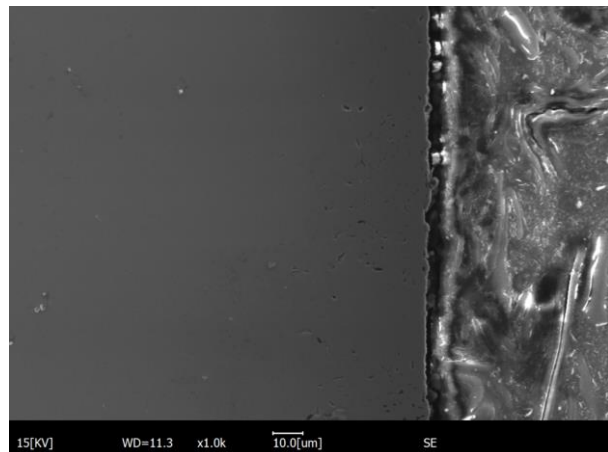


Figure 5. cross-section of the casting specimen after 7 days of corrosion experiment

3-D printed products showed different corrosion behaviors. After the 1-day corrosion experiment, aggressive corrosion was observed through the grain boundaries compared to the inside of the grain (Fig. 6). The specimens without heat treatment showed more severe surface waviness than the specimens with heat treatment.

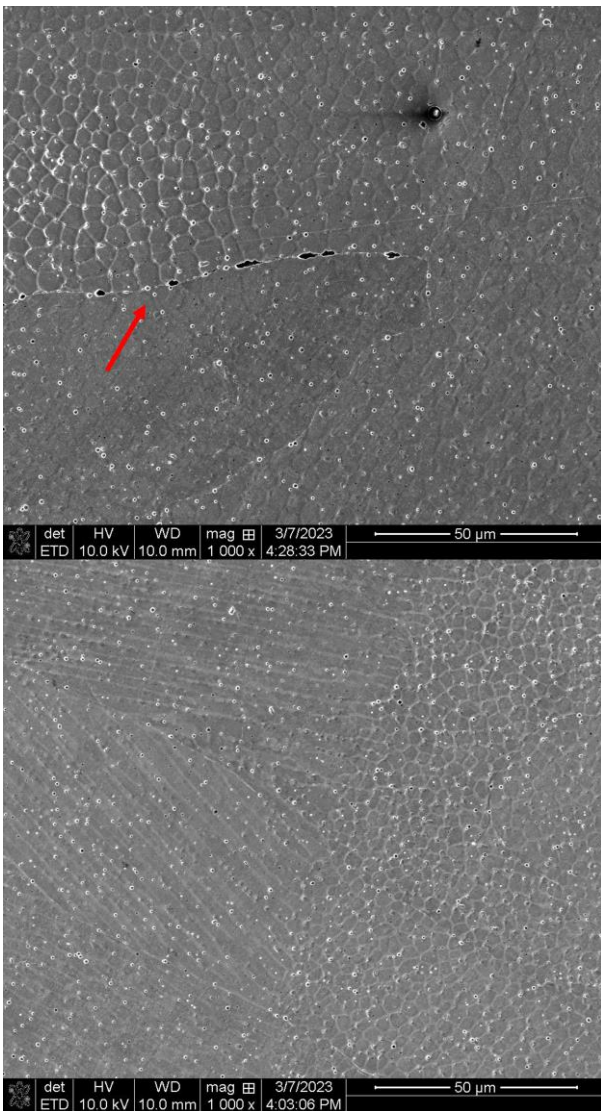


Figure 6. Surface image of 3-D printed alloy without heat treatment (top) and with heat treatment (bottom) after 1-day corrosion experiments.

Especially, on the surface of 3-D printed alloy without heat treatment, vacancies that are predicted to be caused by corrosion were also observed (Fig. 6 (b) red arrow). On the other hand, no voids were found on the surface of the heat-treated specimen. This difference is expected that relatively large grains were recrystallized by the heat treatment and residual stress caused by thermal shock during the manufacturing process was annealed. When observing the cross-section of the 3-D printed specimen after the corrosion experiments, extreme corrosion was observed at the interface of the printed layer rather than inside the printed layer. This is expected that densely developed grain boundaries, which act as the diffusing channel of the corrosive elements of the alloy, enable rapid dissolution of the alloying elements towards the molten salt.

#### 4. Conclusion

Molten salt corrosion behaviors of 80Ni–20Cr alloy which were fabricated by casting and 3-D printing technology were analyzed. Compared to casting products, 3-D printed alloy shows relatively low corrosion resistance to molten salt. Especially, the overlapping region in which micro-grains are located was vulnerable to corrosion. The corrosion rate of thermally treated 3-D printed product was also more aggressive than that of casting although it showed improved corrosion resistance comparing the as-fabricated 3-D printed product. Therefore, it is expected that the development of additional post-treatment techniques for 3-D printed products is essential to use in the molten salt-based application.

#### Acknowledgment

This study was supported by a National Research Foundation of Korea (NRF) grant funded by the Ministry of Science and ICT, Republic of Korea (NRF-2022M2D2A1A02063129).

#### REFERENCES

- [1] Robin Roper, Megan Harkema, Piyush Sabharwall, Catherine Riddle, Brandon Chisholm, Brandon Day, and Paul Marotta, Molten salt for advanced energy applications: A review, *Annals of Nuclear Energy*, Vol. 169, 108924, 2022
- [2] Benito Mignacca, Giorgio Locatelli, Economics and finance of Molten Salt Reactors, *Progress in Nuclear Energy*, Vol. 129, 103503, 2020
- [3] C. Buchanan, L. Gardner, Metal 3D printing in construction: A review of methods, research, applications, opportunities and challenges, *Engineering Structures*, Vol. 180, pp. 332-348, 2019.
- [4] Tuan D. Ngo, Alireza Kashani, Gabriele Imbalzano, Kate T.Q. Nguyen, and David Hui, Additive manufacturing (3D printing): A review of materials, methods, applications and challenges, *Composites Part B: Engineering*, Vol. 143, pp. 172-196, 2018.